From perception to valence: a pair of interneurons that assign positive valence to sweet sensation in *Drosophila*

Kevin William Christie[1,#], Tarandeep Singh Dadyala[1,#], Irina Troufakina Sinakevitch[1], Phuong Chung[2], Masayoshi Ito[2,3], Lisha Shao[1,*]

[1] Department of Biological Sciences, University of Delaware, Newark, DE 19711

[2] Janelia Research Campus, Howard Hughes Medical Institute, Ashburn, VA 20147

[3] Current address: Lib-Gate Co., Tokyo, Japan 105-6923

[#] These authors contributed equally to this work

[*] Correspondence: shaol@udel.edu

Author contributions:

L.S. conceived and supervised the project, conducted calcium imaging, positional preference, and associative learning experiments, and performed connectome analyses. P.C. and L.S. performed the neuroanatomy screen. M.I. generated the split-GAL4 drivers used in the neuroanatomy screen. K.W.C. conducted calcium imaging experiments and performed connectome analyses and model simulations. T.S.D. and I.T.S. performed immunostaining, confocal imaging, and feeding experiments. K.W.C., T.S.D., I.T.S., and L.S. performed data analyses and generated figures. L.S. wrote the manuscript with input from all authors.

Summary

Assigning valence—appeal or aversion—to gustatory stimuli and relaying it to higher-order brain regions to guide flexible behaviors is crucial to survival. Yet the neural circuit that transforms gustatory input into motivationally relevant signals remains poorly defined in any model system. In *Drosophila melanogaster*, substantial progress has been made in mapping the sensorimotor pathway for feeding and the architecture of the dopaminergic reinforcement system. However, where and how valence is first assigned to a taste has long been a mystery. Here, we identified a pair of subesophageal zone interneurons in *Drosophila*, termed Fox, that impart positive valence to sweet taste and convey this signal to the mushroom body, the fly's associative learning center. We show that Fox neuron activity is necessary and sufficient to drive appetitive behaviors and can override a tastant's intrinsic valence without impairing taste quality discrimination. Furthermore, Fox neurons transmit the positive valence to specific dopaminergic neurons that mediate appetitive memory formation. Our findings reveal a circuit mechanism that transforms sweet sensation into a reinforcing signal to support learned sugar responses. The Fox neurons exhibit a convergent–divergent "hourglass" circuit motif, acting as a bottleneck for valence assignment and distributing motivational signals to higher-order centers. This architecture confers both robustness and flexibility in reward processing—an organizational principle that may generalize across species.

Introduction

How sensory information is transformed into emotionally or motivationally charged representations is a central question in neuroscience: Assigning proper valence—appeal or averseness—to sensory stimuli is fundamental for an organism's survival, guiding behaviors such as approach or avoidance, learning, and decision-making. Yet the neural circuits that orchestrate valence assignment across brain regions are unknown or poorly understood.

Conceptually, valence can be viewed as the transformation of a high-dimensional, modality-specific representation (e.g. the taste "sweet") into a lower-dimensional abstract value signal (e.g. "good") that drives flexible behaviors. This valence assignment process depends on a combination

of factors: the stimulus identity and motivational relevance, the animal's internal state, and prior experience. Given its importance for animals' survival, the brain has evolved multiple circuit motifs to implement this computation[1–4]. The taste system exemplifies this complexity because perceived quality and assigned valence can diverge. Sweet taste typically signals energy-rich nutrients and elicits attraction, but it does not invariably produce a rewarding outcome across contexts. Thus, determining whether a taste is "good", "neutral", or "bad" likely requires circuits that integrate context (e.g., concurrent stimuli), internal state (hunger/satiety, metabolic need), and experience (learned associations)—rather than a fixed labeled-line system. For example, fruit flies avoid sugars previously paired with an aversive stimulus[5] and can flip the value of a recently learned sugar cue without changing its sensory identity when ingestion induces post-ingestive malaise signals[6], demonstrating learned reversal of valence. Conversely, flies bearing gut tumors––a drastic alteration in internal state—show reduced aversion to a bitter compound with anti-tumorigenic properties, while avoidance of other bitter tastants remains intact[7] . These examples indicate that taste quality and valence can be dissociated, and that tastant valence can be reweighted by experience and internal physiological states, likely through mechanisms acting downstream of the primary gustatory neurons.

Consistent with this view, emerging evidence indicates that gustatory processing occurs through a layered architecture—early stages encode taste quality in relatively segregated channels (e.g., sweet vs. bitter), whereas downstream stages assign and update valence after integrating the animal's internal state and prior experience[1–4]. Such circuits likely implement convergent and divergent motifs, with specific nodes acting as hubs to route sensory signals into distinct behavioral outputs, from reflexive feeding to reinforcement learning [8–10].

Despite this progress, it remains unclear where along a given gustatory pathway the identity of a taste (e.g., "sweet") is first transformed into a valence that signals "good" or "bad". In mammals, anatomical and functional mapping suggest that this divergence occurs downstream of cortical taste areas—notably in the amygdala and associated hypothalamic/brainstem circuits that drive feeding or avoidance[1] .

In *Drosophila*, a similar organizational logic has been hypothesized, but specific circuit nodes for taste valence assignment have remained elusive. It is well established that the primary gustatory receptor neurons (GRNs) project to the subesophageal zone (SEZ), where they connect to second-order gustatory interneurons (GINs). Recent connectome analyses indicate that most second-order taste neurons in the SEZ remain segregated by modality, mirroring the peripheral labeled lines. By the third-order level, however, taste circuits show increasing convergence and distribute information to multiple brain regions implicated in diverse functions—including regions for feeding motor control, the central olfactory system, and the mushroom body (MB)[10] . In particular, the MB, as the center for associative learning, is innervated by dopaminergic neurons that mediate appetitive reinforcement[11]. This layout suggests that somewhere between the primary sensory neurons and the dopaminergic reinforcement system there exists a critical hub where a taste's valence is first assigned. Identifying that hub—the point at which "sweet" becomes "good" (i.e., rewarding) or "bad" (i.e., aversive)—is crucial for understanding how flexible taste behaviors are implemented at the circuit level.

To elucidate where and how innate valence is assigned and modified to produce flexible behavioral outputs, we must identify the intermediate neuronal layers that transform sensory quality into a hedonic signal. Operationally, neurons that assign valence may share the following properties. (i) Sufficiency—their activation drives appropriate innate response (attraction or aversion) and can serve as a reinforcing signal for learned responses. (ii) Necessity and non-impairment—silencing or removing impairs normal valence-driven behavior without abolishing detection or discrimination of the stimulus. (iii) Override capacity— their activation can, under some conditions, override a stimulus' intrinsic valence (e.g., rendering neutral or aversive taste attractive). In sum, such neurons would encode the hedonic value of the sensory stimulus rather than its identity *per se* [1,8,9,12]. These criteria guided our search for the locus of valence assignment within the fly's gustatory circuitry.

Here, we combine connectome mapping with targeted functional interrogation in the fruit fly, *Drosophila melanogaster*, to pinpoint where the positive valence of tastants first arises within the taste circuitry and how it is relayed to downstream learning circuits. We identified a pair of

SEZ neurons that assign a positive valence to the activity of sweet gustatory neurons. Activating these SEZ neurons is sufficient to drive appetitive behaviors, including approach, proboscis extension, and increased consumption of both food and water.

Crucially, these neurons differ from the sweet gustatory receptor neurons and downstream sensorimotor interneurons in two respects: First, their activation can override a tastant's intrinsic valence, rendering neutral or even aversive tastes attractive. Second, their activation, when paired with a neutral odor cue, drives appetitive olfactory learning. Together, we propose a mechanism by which positive valence is attached to sweet taste inputs and subsequently routed into associative learning networks.

Results

We started searching for neurons in flies whose activation has a valence—rewarding or punishing—by screening 241 restricted-expression split-GAL4 drivers[13] using an optogenetic positional preference assay in which flies choose to prefer or avoid optogenetic neural activation[14] (Figures 1A and S1A). Among the positive hits, one driver line robustly labeled the PPM3 cluster of dopaminergic neurons (DANs) that innervate the fan-shaped body, and, to a lesser extent, a bilateral pair of neurons that innervate the SEZ (Figures S2A and S2B). This piqued our interest because dopaminergic neurons that innervate the mushroom body have been implicated as a key hub for valence processing, analogous to the mammalian cerebellum[12,15]. Unexpectedly, excluding PPM3 DANs from this driver line via genetic intersection (methods in Figure 1B legend) did not abolish the preference; flies still exhibited strong positional preference for the optogenetic activation (fox-ssKZip in Figure 1B). These data implicate the SEZ-innervating neurons—previously named 'Fox' but functionally uncharacterized[16]— as mediating the effect (Figures 1C, 1D, S2A, and S3). Along with two more specific drivers (Figure 1C and S2A), we found that optogenetic activation of Fox neurons induced positional preference, while optogenetic suppression[17] of Fox led to positional aversion (Figure 1B). Together, these findings suggest that Fox neuron activity contributes to valence processing, which prompted us to next investigate their natural function.

Fox activation drives appetitive behaviors

Fox's SEZ location suggested a potential function in feeding-related behaviors. We found that activating Fox neurons significantly promoted proboscis extension reflex (PER) (Figure S1B and S4) and food consumption in the OptoPAD assay[18,19] (Figures 1E, S1E, and S2C). In contrast, blocking Fox neurons, either acutely or chronically, did not significantly affect food consumption (Figures 1E and S5). Intriguingly, activating Fox neurons also promoted consumption of water, although intake nevertheless remained regulated by the duration of dehydration (Figure 1F). Thus, the activation of Fox neurons drives appetitive behaviors, including approaching and preference for Fox neuron activation and increased consumption of food and water.

Fox neurons' phenotypes resemble those of the Feeding (Fdg) neurons, which function as important regulators for feeding behavior[20] and account for 10% of the total synaptic inputs to Fox neurons. Like Fox neurons, activation of Fdg neurons increased food and water consumption and induced acute preference for optogenetic activation (purple bars in Figures 1B, E, and F). This parallel, together with Fox-driven PER (Figure S4), supports the idea that Fox neurons also contribute to the regulation of the feeding sensorimotor program. Connectome analysis showed that, although Fox neurons were not previously classified as higher-order gustatory interneurons (GINs)[4,21] or SEZ local neurons (SEZ-LN)[3] , they receive synaptic inputs from key second- and third-order GINs and project onto premotor neurons controlling PER[21–24] (Figure 2A). Moreover, Fox neurons are a major upstream partner for the drosulfakinin neurons (DSKMP1B; satiety, feeding, and sugar attraction, aggressive and mating arousal regulators in SEZ[25–27]), accounting for over 20% of DSKMP1B synaptic inputs from SEZ. Given that Fox neurons both drive appetitive behaviors and interface with the core feeding pathway[21–24] and internal-state regulators [25–27], we next investigated their role in regulating valence, particularly in the context of sweet taste.

Fox activation overrides the intrinsic valence of taste

To determine whether Fox neurons are sufficient to impose a positive valence on gustatory stimuli, we performed a closed-loop optogenetic feeding assay[19], where starved flies were given a binary choice between two identical probes containing a neutral tastant (agar). Light delivery that drives

neural activation or silencing was coupled in real time with sipping from one designated probe (the associated probe), whereas sipping from the other probe (the non-associated probe) did not trigger light delivery (Figure S1E). This design provides a direct readout of whether neural activity confers positive value to an otherwise neutral stimulus: if activation is rewarding, flies should preferentially return to the associated probe and accumulate more sips there.

Consistent with this prediction, flies took significantly more sips from the probe associated with activation of Fox, Fdg, or Gr64f-expressing sweet GRNs compared to the non-associated probe, indicating that activating each of these cell types can endow a neutral tastant with positive value (Figure 2B, i). To facilitate cross-cell-type comparison, we quantified preference as the difference between sips on associated versus non-associated probe, normalized by the total sips: $(Sip_{ON}-Sip_{OFF})/Sip_{Total}$ (Figure 2B, ii). By construction, this metric controls for inter-fly variability in total consumption and centers chance performance at 0. In line with the sip counts, activating any of these neurons increased flies' preference for the associated probe. In contrast, pairing the probe with optogenetic silencing of Fox neurons did not produce preference for either probe (blue bars in Figure 2B). Together, these results demonstrate that Fox activation is sufficient to impose positive valence on a neutral tastant.

We next tested whether Fox activation could override aversive valence. Replacing the neutral tastant with an innately bitter compound (0.5 mM quinine in agar) strongly limits intake under baseline conditions. In this setting, activation of Gr64f or Fdg neurons supported only minimal intake (~100 sips total) and yielded, at most, a marginal bias toward the associated probe (Figure 2C). In contrast, activation of Fox neurons drove ~1000 sips—an order-of-magnitude increase relative to Gr64f or Fdg activation—and produced a significantly higher preference for the associated probe (Figure 2C). Thus, Fox activation can surmount the aversive impact of quinine to promote both approach and persistent intake.

To dissect Fox-mediated valence assignment, we asked whether Fox activation promotes bitter intake even in fed flies that lack a strong drive to consume quinine. We found that activating Fox neurons—but not Fdg—significantly increased quinine consumption in fed animals (Figure 2D).

Furthermore, the Fox-induced increase in consumption scaled inversely with quinine concentration: as bitterness increased, the consumption gain driven by Fox activation decreased (Figure 2D). This graded response argues against a purely compulsive, hardwired feeding command and instead supports a model in which Fox acts downstream of the sensorimotor feeding pathway to modulate hedonic value—amplifying the attractiveness of the ingested stimulus in a manner that remains sensitive to stimulus quality.

In sum, Fox neurons share with elements of the sweet sensorimotor pathway the capacity to engage the feeding program (as supported by consumption data and our connectome analysis in Figure 2A), but diverge functionally from sweet GRN/GIN pathways in their ability to overcome negative taste valence. Fox activation overrides the inherent neutral or aversive valence of tastants and can reduce dependence on hunger-state gating, indicating that Fox neurons operate downstream of primary taste identity/perception to assign positive valence to gustatory stimuli and sustain consummatory behavior.

Fox silencing impairs taste valence without altering taste identity

We next assessed whether Fox is essential for the valence associated with gustatory stimuli by examining taste-driven behaviors in the absence of Fox function. First, we asked whether Fox is required for the appetitive effect normally driven by sweet-GRN activation. Silencing Fox abolished the increase in food consumption elicited by activating Gr64f-expressing GRNs (Figure 3A). In the closed-loop assay that paired Gr64f activation with designated probe, Fox silencing did not change the normalized preference (Figure 3B, ii) but eliminated the absolute consumption advantage at the associated probe: sip counts at the associated and non-associated probes became indistinguishable (Figure 3B, i). Together, these findings indicate that silencing Fox neurons impairs the appetitive responses driven by sweet-GRN activation.

We then asked whether this impairment reflects a failure to assign valence or a deficit in detecting taste identity. We formulated two hypotheses—identity vs valence—and made explicit predictions for two-choice discrimination (sucrose vs agar; sucrose vs quinine) under both Fox activation and silencing.

If Fox encodes sweet identity: (i) Activation should render both options more sweet-like, thereby reducing discriminability (preference drifts toward 0) because the identity contrast diminishes. (ii) When fox is silenced, Gr64f activation should not restore sucrose preference because identity cannot be read out downstream. Hence, silencing should diminish discrimination (i.e., preference toward 0).

If Fox assigns positive valence downstream of identity: (i) Activation should increase sucrose-over-agar and sucrose-over-quinine preference (though the effect may be limited when sucrose preference is already near maximal (e.g., physical limits on sip counts)). An increase is more likely observed in sucrose vs quinine, where high contrast may allow nonlinear amplification of the positive option; this is especially evident when total sip counts are relatively low due to bitter-induced feeding suppression. (ii) Silencing should preserve direction (sucrose still preferred over agar or quinine) but reduce the magnitude of the choice (i.e., weaker preference).

Overall, our data support the valence hypothesis. Fox-silenced flies continued to differentiate sweet from neutral or bitter tastants, exhibiting positive choice scores across all conditions tested (Figures 3C-F), demonstrating intact taste identity. In line with our predictions, in sucrose-agar experiment, neither Fox activation nor silencing altered sucrose preference relative to no-LED controls (Figure 3C), consistent with a ceiling constraint: upon Fox activation, flies took >3,000 sips from sucrose (Figure 3C, i), leaving little room for further increase and thus no change in the normalized preference index (Figure 3C, iii) By contrast, in sucrose-quinine experiment, Fox activation increased sucrose preference and Fox silencing reduced it (Figure 3D)—exactly as predicted if Fox scales an already positive option (sucrose) widens the gap against a negative option (quinine), while removing the valence amplifier narrows that gap. The asymmetry between the two discrimination contexts (sucrose-agar vs sucrose-quinine) is therefore consistent with nonlinear valence amplification and with dynamic-range limits in the sucrose-agar setting. Together, these results support the valence hypothesis and indicate that Fox may not add a fixed value offset but instead scale positive valence, with effect size depending on stimulus contrast and available behavior dynamic range.

Constitutive Fox silencing with Kir2.1 likewise produced preferences for sucrose over agar or quinine comparable to genetic controls (Figures 3E-F), reinforcing the conclusion that sweet identity is preserved without Fox. The partial divergence from the optogenetic silencing phenotype in the sucrose vs quinine condition (Figure 3D) likely reflects developmental and/or homeostatic compensation under chronic silencing, a common outcome in constitutive manipulations.

Consistent with a downstream role of Fox, activating Gr64f sweet-GRNs did not change sucrose-over-quinine preference, with or without constitutive Fox silencing via Kir2.1 (Figure 3G). Crucially, Fox-silenced flies still displayed net sucrose preference and quinine aversion (Figures 3D and 3F), confirming that sweetness and bitterness detection remain intact despite disrupted hedonic scaling.

In sum, Fox neurons are necessary to express full positive, valence-specific feeding responses (e.g., the Gr64f-evoked consumption increase), but not for taste identity per se, which is supported by the GRN–GIN pathway. These results place Fox downstream of primary taste identity/perception as an integrator that generates positive valence from gustatory stimuli.

Fox neurons are essential for appetitive learning induced by GRN activation

In a standard associative learning paradigm, flies learn to associate a neutral odor (conditioned stimulus, CS) with a rewarding sweet tastant (unconditioned stimulus, US), and memory strength is quantified as the proportion of flies staying in proximity to the source of the US-paired odor[28,29] . In a variation of this assay, optogenetic activation of sweet GRNs can substitute for natural sweet tastants, serving as an artificial US to drive learning[30] . This substitution approach allows us to probe how specific neurons contribute to associative memory formation. We hypothesized that Fox neurons function as a critical node in generating positive valence and subsequently conveying it to the brain's associative learning center.

Consistent with this hypothesis, pairing an odor with optogenetic activation of Fox neurons produced robust appetitive memory (Figure 4A), whereas optogenetic suppression of Fox—despite eliciting acute aversion in the positional preference assay (Figure 1B)—did not form an aversive

memory in the learning assay (Figure 4A). Notably, activating Fdg neurons failed to generate appetitive learning (purple bar in Figure 4A). Moreover, none of the other key GINs that connect to Fox—Clavicle, Rattle, FMIn, Bract, and Roundup[21] —generated appetitive olfactory memory when their activation was paired with odors in a recent study[4].

We next tested whether Fox neurons are required for appetitive learning driven by natural sugar stimulus, which is mediated by sweet GRNs and conveyed to the learning center. Starved flies formed robust appetitive memory with odors paired with sucrose, whereas silencing Fox significantly reduced this memory (Figure 4B). To test if Fox neurons mediate the valence of sweet-GRN activation specifically, we paired odor with activation of Gr64f-expressing sweet-GRNs while simultaneously blocking Fox neural activity. We found that blocking Fox neurons significantly compromised the learning generated by Gr64f-GRN activation (Figure 4C), indicating that Fox is required downstream of sweet GRNs that mediate the sugar induced appetitive memory formation. The results of our learning experiments differentiate Fox neurons from the sensorimotor pathway for feeding in the context of associative learning.

Because Fox is necessary for sucrose- and sweet-GRN-induced learning, we hypothesized that Fox receives input from sweet GRNs. To test this, we performed a functional connectivity assay using two-photon calcium imaging. Briefly, we optogenetically stimulated Gr64f-expressing sweet GRNs while recording calcium signals from Fox neurons. Fox projections exhibited significant calcium responses to Gr64f stimulation (Figure 4D), suggesting that Fox neurons receive input from peripheral sweet GRNs.

Taken together, these results suggest that Fox activity is sufficient to substitute the unconditioned stimulus to support appetitive learning and necessary for appetitive learning induced by both natural sugar and sweet-GRN activation. We conclude that Fox acts as a key relay that transforms sweet GRN activity into positive valence and delivers this signal to the associative learning center.

Fox neurons connect to the learning center via ascending downstream neurons

Our results raise the question of how tastant valence is assigned and relayed to the central brain, particularly the learning center. For example, it is well characterized that appetitive gustatory inputs activate the Protocerebral Anterior Medial cluster of dopaminergic neurons (PAM-DANs) that innervate the horizontal lobes of the mushroom body. The changes in PAM-DANs' activity in turn modify the synaptic plasticity between mushroom body intrinsic neurons and output neurons, in a compartment-specific manner[11,15,31,32] , producing learned behavioral changes.

Connectome analysis revealed that Fox neurons connect to PAM-DANs via 11 pairs of ascending downstream neurons (termed as Fox Downstream Ascending, FDA, neurons; Figure 5J; full list and synaptic connectivity in Table S2A). Three FDA pairs synapse directly onto PAM-DANs (FDA-I) and have previously been shown to be critical for appetitive learning[33], whereas the remaining pairs lie one synapse upstream of PAM-DANs (FDA-II). Across Fox output, FDA-I and FDA-II account for 4.4% and 10.5% of total Fox synaptic output, respectively.

To test whether Fox neurons function as a node that links sweet-sensing GRNs to PAM-DANs through FDA neurons, we performed a computational simulation[34] using a leaky integrate-and-fire model based on the *Drosophila* whole brain connectome[21,23,35]. We simulated unilateral activation of labellar sweet-sensing GRNs at various frequencies and model synaptic weights. As expected, the number of responsive PAM-DANs increased monotonically with stronger GRN stimulation frequencies and model synaptic weights (Figure 5A and S6A "Fox intact" panel; Table S3). In contrast, silencing Fox neurons in the model almost completely abolished PAM-DAN firing across conditions (Figure 5A and S6A, "Fox silenced" panel; Table S3). We next silenced FDA neurons individually and in groups.

Computational silencing FDA-I, FDA-II, or all FDA neurons simultaneously significantly reduced the PAM-DANs response to GRN stimulation (Figure 5B; Table S2B). Notably, silencing CB0233—an FDA-II neuron pair that accounts for 7% of total Fox synaptic output and 41% of Fox output to FDA neurons (Figure S2) —was sufficient on its own to block PAM-DAN response *in silico* (Figure 5B; Table S2B). These simulations yielded two predictions: (i) blocking downstream ascending (FDA)

neurons should compromise appetitive behaviors and learning, mirroring Fox silencing. (ii) Fox neurons should be functionally connected to PAM-DANs.

We then tested these predictions experimentally, focusing on CB0233 given its dominant share of Fox→FDA output. We found that activating CB0233 did not promote food consumption or generate appetitive memory when paired with odor (Figure 5C-D). However, blocking CB0233 abolished Gr64f-induced increase in feeding (Figure 5E) and Gr64f-induced appetitive learning (Figure 5F), recapitulating the effect of Fox silencing on Gr64f-induced feeding and learning (Figure 3A and 4C). Thus, while activation of CB0233 alone is not sufficient to drive feeding or conditioned preference, CB0233 is required for the GRN→Fox-dependent enhancement of feeding and appetitive memory, indicating that it is a major postsynaptic target of Fox that relays positive valence toward the learning center along with other FDA neurons.

To test the functional connection between Fox and PAM-DANs directly, we conducted a two-photon calcium imaging assay in which we optogenetically stimulated Fox while recording from PAM-DANs. Fox stimulation activated PAM-DANs innervating the MB γ4, γ5, β2, and β'2 compartments (Figure 5G), regions essential for appetitive olfactory learning[11,15] . Finally, to test whether the connection between Fox and PAM-DANs can shape behaviors, we performed a neural epistasis experiment: activating Fox while optogenetically blocking PAM-DANs. We found that blocking PAM-DANs did not affect the Fox-induced increased in food consumption (Figure 5H) but completely abolished the appetitive learning produced by Fox activation (Figure 5I). These results place Fox upstream of PAM-DANs for learning, while indicating that Fox-driven feeding increases can proceed via PAM-independent pathways.

In sum, Fox serves as a shared early node from which the feeding motor program and the valence/learning pathways bifurcate. Fox assigns and relays the positive valence from sweet-GRN activity to the PAM-DANs and the mushroom body via its ascending downstream (FDA) neurons.

Discussion

In this study, we identified a pair of SEZ neurons in *Drosophila*, termed Fox, as a hub that links sweet GRN input to appetitive learning circuits. Our imaging and behavioral data support a working model in which Fox neurons assign and relay the positive valence of sweet GRN activity to PAM-DANs via its downstream neurons to facilitate learning, thereby effectively bridging peripheral taste detection and central reinforcement pathways[15,31] (Figure 5J).

This model is supported by several complementary lines of evidence: (i) Sufficiency for reward: acute activation of Fox is perceived as rewarding—it drives appetitive behaviors and serves as a positive reinforcer in olfactory conditioning (Figures 1B, 1E, 1F and 4A). (ii) State-sensitive scaling, not compulsion: Fox activation increases food, water, and quinine intake even in fed flies, yet the magnitude of these effects remains gated by deprivation level and bitterness (Figures 1E, 1F, 2D), indicating that the Fox-evoked appetitive drive is homeostatically regulated rather than a compulsive motor program. (iii) Valence override downstream of sensorimotor control: Fox activation can override intrinsic neutral or aversive tastant valence of otherwise unpalatable or bitter tastants—even in fed flies with low drive—consistent with a site downstream of the feeding sensorimotor pathway where dependence on hunger gating is reduced (Figures 2B-D). (iv) Necessity for sweet-driven appetitive response with identity preserved: silencing Fox impairs sweet-GRN-driven consumption increase without compromising the recognition of taste identity (Figures 3A-F). Notably, Fox activation increases, whereas Fox silencing decreases, sucrose-over-quinine choice (Figure 3D); this suggests a nonlinear valence scaling—enhancing "good" tastes more than diminishing "bad" tastes (making "good" better and "bad" less bad)—rather than encoding sensory identity. (v) Position in the sugar→GRN→Fox→FDA→learning chain: Fox receives functional input from sweet GRNs (Figure 4D), is required for sucrose-induced learning (Figure 4B), and its downstream FDA neurons are necessary for GRN-driven feeding and memory (blocking a single pair, CB0233, phenocopies Fox loss for Gr64f-evoked behaviors; Figures 4C, 5F). (vi) Relay to reinforcement compartments: Fox stimulation activates PAM-DANs that innervate MB γ4/γ5/β2/β'2 compartments (Figure 5G), and blocking PAM-DANs abolishes Fox-driven appetitive learning while sparing Fox-driven consumption (Figures 5I and 5H). Together, these results show that Fox

activity confers a positive valence to tastants, not sensory detection. Furthermore, our results delineate a GRN→Fox→FDA→PAM pathway for sugar-induced appetitive learning and place Fox upstream of PAM-DANs for reinforcement while permitting PAM-independent increases in feeding.

At the circuit level, this working model supports a convergent–divergent motif centered on Fox. Multiple sweet GRNs and higher-order GINs converge onto Fox neurons, and Fox outputs diverge to multiple targets: premotor targets and ascending pathways. Functionally, Fox behaves as an SEZ bottleneck that likely requires convergent drive (and/or specific temporal patterns) to reach threshold, consistent with selective recruitment. Downstream of Fox, we propose two partially separable routes (Figure 5J). (i) A premotor/feeding route—dominated by SEZ interneurons together with FDA neuron CB0233—that provides short-latency access to premotor and motor neurons, accounting for the increased feeding with GRN→Fox activation. (ii) An ascending valence route that recruits MB-innervating PAM-DANs for reinforcement during learning. Although CB0233 carries a large fraction of Fox output to FDAs, it does not directly synapse onto PAM-DANs. Accordingly, CB0233 activation alone is insufficient for feeding or memory, yet CB0233 is required for GRN→Fox-supported enhancement of both.

Exploratory computational simulations showed that silencing Fox neurons and/or FDA neurons suppressed the widespread network responsiveness to GRN stimulation (Figure S6C and Table S4). This effect was not observed when silencing higher-order GINs (Figure S6D) or SEZ cholinergic "Fox-like" neurons with a similar bilateral morphology (Figure S6E and Table S4; "Fox-like" definition in legend), indicating a unique circuitry characteristic in Fox. These simulations, together with the anatomy, point to an "hourglass" organization: diverse sweet signals funnel through a unified hedonic assignment node before distribution—a design that confers both consistency and flexibility.

After this bottleneck, reward signals are distributed to separate downstream networks governing memory and feeding. Connectome analyses place Fox among the "balanced rich-club" neurons that efficiently integrate and disseminate information[36] and identify Fox as the only SEZ local

input to the Interoceptive SEZ Neuron (ISN), a “rich-club broadcaster” neuron[36]. Fox downstream neurons project broadly, especially to the superior medial and lateral protocerebrum (Figures S3F and 5J). This organization suggests that distinct Fox-downstream channels relay Fox activity to specialized regions. Beyond specific PAM-DANs and typical mushroom body output neurons (MBONs; e.g., MBON1, MBON14) implicated in learning[31] , Fox also connects with PPL1 DANs and atypical MBONs (e.g., MBON35) that may route learned valence into premotor systems[37]. Moreover, Fox is a major SEZ input to DSK neurons (DSKMP1B), which regulate internal states (satiety, aggressiveness, and sexual arousal)[26,38,39]. We therefore hypothesize that state signals (e.g., DSK) modulate Fox excitability at the bottleneck, scaling appetitive value according to need.

Such hourglass architectures recur across taxa: in mammals, for example, gustatory inputs from multiple peripheral fibers converge in the parabrachial nucleus before projecting to hypothalamic, amygdalar, and cortical targets involved in feeding and learning[40,41]. Such architectures—whether in insects or mammals—underlie the ability of organisms to distill complex sensory information into a unifying affective code that can drive coherent adaptive behaviors.

Our research also opens several important questions for future research. First, modality scope. Are Fox functions specific to sugar, or do they extend to other taste modalities (e.g., umami)? Connectome analyses indicate that protein and bitter GRNs connect to Fox neurons within 2-3 synapses. Testing how Fox integrates across modalities and interacts with negative-valence pathways will clarify its role in valence assignment. Second, non-gustatory inputs and state control: Identifying non-gustatory inputs to Fox (e.g., hormonal or neuromodulator signals) will reveal how internal state dynamically tunes the bottleneck to reshape valence computation.

In summary, we propose that the Fox circuitry represents a mechanism through which positive valence is attached to gustatory input and conveyed to the central brain. Fox functions as a specialized SEZ hub that transforms sweet identity into value, distributes that signal to reinforcement circuits for learning and to premotor pathways for feeding, and likely integrates internal state to modulate appetitive drive. These findings reveal the neural basis of reward, motivation, and behavioral flexibility in the face of changing environments and needs.

Acknowledgements

We thank Dr. Ulrike Heberlein for her support during early stages of this project and her feedback on the manuscript. We thank Yoonwoo Park and Sabina Knox for their contributions to the early stage of this project. We thank Dr. Nicholas Collins and Madison Endres for their assistance with fly work. We thank Drs. Jon-Michael Knapp, Karla Kaun, Yichun Shuai, Yoshi Aso, and Yufeng Pan for discussion and feedback. We thank Drs. Daniel Bushey, Glenn Turner, Mehrab Modi, Yoshi Aso, and Vasily Goncharov for technical support and advice. We are grateful to Dr. Key Ito, Yichun Shuai, Daniel Bushey, Glenn Turner, Yoshi Aso, Karla Kaun, Anita Devineni, Gabriella Sterne, Mark Wu, the HHMI Janelia Research Campus, and Bloomington *Drosophila* Stock Center (BDSC) for providing fly strains. We thank Dr. Philip Shiu for publicly sharing code for brain simulations and providing advice on implementation. We acknowledge the Princeton FlyWire team and members of the Murthy and Seung labs for development and maintenance of FlyWire (supported by BRAIN Initiative grant MH117815 to Murthy and Seung). This work was supported by UD-GUR, UD-UDRF, Delaware CTR program with a grant from the National Institute of General Medical Sciences (NIGMS, U54 GM104941), Delaware INBRE program with a grant from the NIGMS (P20 GM103446), and Maximizing Investigators' Research Award to L.S. (NIGMS R35GM147504).

References

1. Wang L, Gillis-Smith S, Peng Y, et al. The coding of valence and identity in the mammalian taste system. *Nature*. 2018;558(7708):127-131. doi:10.1038/s41586-018-0165-4

2. Jin H, Fishman ZH, Ye M, Wang L, Zuker CS. Top-Down Control of Sweet and Bitter Taste in the Mammalian Brain. *Cell*. 2021;184(1):257-271.e16. doi:10.1016/j.cell.2020.12.014

3. Li J, Dhaliwal R, Stanley M, Junca P, Gordon MD. Functional imaging and connectome analyses reveal organizing principles of taste circuits in Drosophila. *Curr Biol*. Published online 2025. doi:10.1016/j.cub.2025.04.035

4. Jacobs RV, Wang CX, Nguyen L, et al. Overlap and divergence of neural circuits mediating distinct behavioral responses to sugar. *Cell Rep*. 2024;43(10):114782. doi:10.1016/j.celrep.2024.114782

5. Masek P, Scott K. Limited taste discrimination in Drosophila. *Proceedings of the National Academy of Sciences of the United States of America*. 2010;107(33):14833-14838. doi:10.1073/pnas.1009318107

6. Senapati B, Treiber CD, Waddell S. Visceral signaling of post-ingestive malaise directs memory updating in Drosophila. Published online 2025. doi:10.1101/2025.10.21.683769

7. Leung NY, Xu C, Li JSS, et al. Gut tumors in flies alter the taste valence of an anti-tumorigenic bitter compound. *Curr Biol*. 2024;34(12):2623-2632.e5. doi:10.1016/j.cub.2024.04.082

8. Tye KM. Neural Circuit Motifs in Valence Processing. *Neuron*. 2018;100(2):436-452. doi:10.1016/j.neuron.2018.10.001

9. Burton TJ, Balleine BW. The positive valence system, adaptive behaviour and the origins of reward. *Emerg Top Life Sci*. 2022;6(5):501-513. doi:10.1042/etls20220007

10. Walker SR, Peña-Garcia M, Devineni AV. Connectomic analysis of taste circuits in Drosophila. *Sci Rep*. 2025;15(1):5278. doi:10.1038/s41598-025-89088-9

11. Aso Y, Rubin GM. Dopaminergic neurons write and update memories with cell-type-specific rules. *eLife*. 2016;5:156. doi:10.7554/elife.16135

12. Aso Y, Sitaraman D, Ichinose T, et al. Mushroom body output neurons encode valence and guide memory-based action selection in Drosophila. *eLife*. 2014;3:e04580. doi:10.7554/elife.04580

13. Meissner GW, Vannan A, Jeter J, et al. A split-GAL4 driver line resource for Drosophila neuron types. *eLife*. 2025;13:RP98405. doi:10.7554/elife.98405

14. Shao L, Saver M, Chung P, et al. Dissection of the Drosophila neuropeptide F circuit using a high-throughput two-choice assay. *Proceedings of the National Academy of Sciences of the United States of America*. 2017;114(38):E8091-E8099. doi:10.1073/pnas.1710552114

15. Modi MN, Shuai Y, Turner GC. The Drosophila Mushroom Body: From Architecture to Algorithm in a Learning Circuit. *Annual review of neuroscience*. 2020;43(1):465-484. doi:10.1146/annurev-neuro-080317-0621333

16. Sterne GR, Otsuna H, Dickson BJ, Scott K. Classification and genetic targeting of cell types in the primary taste and premotor center of the adult Drosophila brain. *eLife*. 2021;10:e71679. doi:10.7554/elife.71679

17. Bushey D, Shiozaki H, Shuai Y, et al. RubyACRs Enable Red-Shifted Optogenetic Inhibition in Freely Behaving Drosophila. *bioRxiv*. Published online 2025:2025.06.13.659144. doi:10.1101/2025.06.13.659144

18. Itskov PM, Moreira JM, Vinnik E, et al. Automated monitoring and quantitative analysis of feeding behaviour in Drosophila. *Nat Commun*. 2014;5(1):4560. doi:10.1038/ncomms5560

19. Moreira JM, Itskov PM, Goldschmidt D, et al. optoPAD, a closed-loop optogenetics system to study the circuit basis of feeding behaviors. *eLife*. 2019;8:e43924. doi:10.7554/elife.43924

20. Flood TF, Iguchi S, Gorczyca M, White B, Ito K, Yoshihara M. A single pair of interneurons commands the Drosophila feeding motor program. *Nature*. 2013;499(7456):83-87. doi:10.1038/nature12208

21. Shiu PK, Sterne GR, Engert S, Dickson BJ, Scott K. Taste quality and hunger interactions in a feeding sensorimotor circuit. *eLife*. 2022;11:e79887. doi:10.7554/elife.79887

22. Dorkenwald S, Matsliah A, Sterling AR, et al. Neuronal wiring diagram of an adult brain. *Nature*. 2024;634(8032):124-138. doi:10.1038/s41586-024-07558-y

23. Schlegel P, Yin Y, Bates AS, et al. Whole-brain annotation and multi-connectome cell typing of Drosophila. *Nature*. 2024;634(8032):139-152. doi:10.1038/s41586-024-07686-5

24. Walker SR, Peña-Garcia M, Devineni AV. Connectomic analysis of taste circuits in Drosophila. *bioRxiv*. Published online 2024:2024.09.14.613080. doi:10.1101/2024.09.14.613080

25. Söderberg JAE, Carlsson MA, Nässel DR. Insulin-Producing Cells in the Drosophila Brain also Express Satiety-Inducing Cholecystokinin-Like Peptide, Drosulfakinin. *Front Endocrinol*. 2012;3:109. doi:10.3389/fendo.2012.00109

26. Guo D, Zhang YJ, Zhang S, et al. Cholecystokinin-like peptide mediates satiety by inhibiting sugar attraction. *PLoS Genet*. 2021;17(8):e1009724. doi:10.1371/journal.pgen.1009724

27. Nässel DR, Zandawala M. Endocrine cybernetics: neuropeptides as molecular switches in behavioural decisions. *Open Biol*. 2022;12(7):220174. doi:10.1098/rsob.220174

28. Krashes MJ, DasGupta S, Vreede A, White B, Armstrong JD, Waddell S. A neural circuit mechanism integrating motivational state with memory expression in Drosophila. *Cell*. 2009;139(2):416-427. doi:10.1016/j.cell.2009.08.035

29. Krashes MJ, Waddell S. Drosophila appetitive olfactory conditioning. *Cold Spring Harbor protocols*. 2011;2011(5):pdb.prot5609-pdb.prot5609. doi:10.1101/pdb.prot5609

30. Shuai Y, Sammons M, Sterne GR, et al. Driver lines for studying associative learning in Drosophila. *eLife*. 2025;13:RP94168. doi:10.7554/elife.94168

31. Aso Y, Hattori D, Yu Y, et al. The neuronal architecture of the mushroom body provides a logic for associative learning. *eLife*. 2014;3:e04577. doi:10.7554/elife.04577

32. Boto T, Stahl A, Tomchik SM. Cellular and circuit mechanisms of olfactory associative learning in Drosophila. *J Neurogenet*. 2020;34(1):36-46. doi:10.1080/01677063.2020.1715971

33. Otto N, Pleijzier MW, Morgan IC, et al. Input Connectivity Reveals Additional Heterogeneity of Dopaminergic Reinforcement in Drosophila. *Curr Biol*. 2020;30(16):3200-3211.e8. doi:10.1016/j.cub.2020.05.077

34. Shiu PK, Sterne GR, Spiller N, et al. A Drosophila computational brain model reveals sensorimotor processing. *Nature*. 2024;634(8032):210-219. doi:10.1038/s41586-024-07763-9

35. Dorkenwald S, Matsliah A, Sterling AR, et al. Neuronal wiring diagram of an adult brain. *bioRxiv*. Published online 2023:2023.06.27.546656. doi:10.1101/2023.06.27.546656

36. Lin A, Yang R, Dorkenwald S, et al. Network statistics of the whole-brain connectome of Drosophila. *Nature*. 2024;634(8032):153-165. doi:10.1038/s41586-024-07968-y

37. Li F, Lindsey JW, Marin EC, et al. The connectome of the adult Drosophila mushroom body provides insights into function. *eLife*. 2020;9:e62576. doi:10.7554/elife.62576

38. Nässel DR, Wu SF. Cholecystokinin/sulfakinin peptide signaling: conserved roles at the intersection between feeding, mating and aggression. *Cell Mol Life Sci*. 2022;79(3):188. doi:10.1007/s00018-022-04214-4

39. Wu S, Guo C, Zhao H, et al. Drosulfakinin signaling in fruitless circuitry antagonizes P1 neurons to regulate sexual arousal in Drosophila. *Nat Commun*. 2019;10(1):4770. doi:10.1038/s41467-019-12758-6

40. Fu O, Iwai Y, Kondoh K, Misaka T, Minokoshi Y, Nakajima K ichiro. SatB2-Expressing Neurons in the Parabrachial Nucleus Encode Sweet Taste. *Cell Rep*. 2019;27(6):1650-1656.e4. doi:10.1016/j.celrep.2019.04.040

41. Nagashima T, Mikami K, Tohyama S, Konno A, Hirai H, Watabe AM. State-dependent modulation of positive and negative affective valences by a parabrachial nucleus-to-ventral tegmental area pathway in mice. *Front Neural Circuits*. 2023;17:1273322. doi:10.3389/fncir.2023.1273322

42. Xie T, Ho MCW, Liu Q, et al. A Genetic Toolkit for Dissecting Dopamine Circuit Function in Drosophila. *Cell reports*. 2018;23(2):652-665. doi:10.1016/j.celrep.2018.03.068

43. Klapoetke NC, Murata Y, Kim SS, et al. Independent Optical Excitation of Distinct Neural Populations. *Nat methods*. 2014;11(3):338-346. doi:10.1038/nmeth.2836

44. Pfeiffer BD, Ngo TTB, Hibbard KL, et al. Refinement of Tools for Targeted Gene Expression in Drosophila. *Genetics*. 2010;186(2):735-755. doi:10.1534/genetics.110.119917

45. Zhang Y, Rózsa M, Liang Y, et al. Fast and sensitive GCaMP calcium indicators for imaging neural populations. *Nature*. 2023;615(7954):884-891. doi:10.1038/s41586-023-05828-9

46. Strother JA, Wu ST, Wong AM, et al. The Emergence of Directional Selectivity in the Visual Motion Pathway of Drosophila. *Neuron*. 2017;94(1):168-182.e10. doi:10.1016/j.neuron.2017.03.010

47. Stimberg M, Brette R, Goodman DF. Brian 2, an intuitive and efficient neural simulator. *eLife*. 2019;8:e47314. doi:10.7554/elife.47314

48. Schindelin J, Arganda-Carreras I, Frise E, et al. Fiji: an open-source platform for biological-image analysis. *Nat Methods*. 2012;9(7):676-682. doi:10.1038/nmeth.2019

49. Shell BC, Schmitt RE, Lee KM, et al. Measurement of solid food intake in Drosophila via consumption-excretion of a dye tracer. *Scientific reports*. 2018;8(1):11536. doi:10.1038/s41598-018-29813-9

50. Shao L, Chung P, Wong A, et al. A Neural Circuit Encoding the Experience of Copulation in Female Drosophila. *Neuron*. 2019;102(5):1025-1036.e6. doi:10.1016/j.neuron.2019.04.009

Materials and Methods

Key resources table

Reagent type (species or re-source)	Designation	Source	Identifier
Genetic reagent (*D. melanogaster*)	Fox-ss1: 26H07-AD(attP40);VT033647-DBD(attP2)	This paper	N/A
Genetic reagent (*D. melanogaster*)	fox-ssKZip: 26H07-AD(attP40),TH-D-KZip+; VT033647-DBD(attP2)	This paper	N/A
Genetic reagent (*D. melanogaster*)	TH-D-Kzip+	Xie *et al.*, 2018[42]	N/A
Genetic reagent (*D. melanogaster*)	fox-l3: Dfd-AD, VT033647-DBD/TM6B	Sterne *et al.,* 2021[16]	N/A
Genetic reagent (*D. melanogaster*)	UAS-CsChrimson-mVenus (attP18)	Klapoetke *et al.*, 2014[43]	BDSC: 55134
Genetic reagent (*D. melanogaster*)	UAS-A1ACR-EYFP (attP18)	Bushey *et al.,* 2025[17]	N/A
Genetic reagent (*D. melanogaster*)	Fdg: SS46913	Sterne *et al.,* 2021[16]	BDSC:87380
Genetic reagent (*D. melanogaster*)	UAS-Kir2.1	Baines *et al.,* 2001	BDSC: 6595
Genetic reagent (*D. melanogaster*)	UAS-Kir2.1-eGFP (attP2)	Y. Shuai	N/A
Genetic reagent (*D. melanogaster*)	R58E02-LexA (attP40)	Pfeiffer *et al.,* 2010[44]	BDSC: 52740

Genetic reagent (*D. melanogaster*)	Gr64f-LexA	Y. Shuai	N/A
Genetic reagent (*D. melanogaster*)	LexAop-CsChrimson88-tdTomato (attP18)	Y. Shuai	N/A
Genetic reagent (*D. melanogaster*)	LexAop-jGCaMP7s (Su(Hw)attP8)	A. Wong	N/A
Genetic reagent (*D. melanogaster*)	UAS-RSET-jGCaMP8s (Su(Hw)attP5)	Zhang et al., 2023[45]	BDSC: 605078
Genetic reagent (*D. melanogaster*)	UAS-Chrimson88-tdTomato (attP18)	Strother *et al.,* 2017[46]	N/A
Antibody	Rabbit anti-GFP	Invitrogen	A-6455
Antibody	Mouse nc82	Hybridoma Bank DSHB	NC82
Antibody	Alexa 568 goat anti-mouse	Invitrogen	A-11031
Antibody	Alexa 488 goat anti-rabbit	Invitrogen	A-11008
Chemicals	Bovine serum albumin (BSA)	Sigma-Aldrich	A7906
Chemicals	Calcium chloride	Sigma-Aldrich	793639
Chemicals	D-glucose	Sigma-Aldrich	G5767
Chemicals	Magnesium chloride, hexahydrate	Sigma-Aldrich	M9272
Chemicals	Normal goat serum	Gibco	16210-064
Chemicals	Paraformaldehyde, 20% aqueous solution	Electron Microscopy Sciences	15713

Chemicals	Phosphate buffer saline (10X)	Apex BioRe-search	18-244
Chemicals	Potassium chloride	Sigma-Aldrich	P9333
Chemicals	Quinine hydrochloride dihydrate	Sigma-Aldrich	22630
Chemicals	Schneider's *Drosophila* medium	Gibco	21720-024
Chemicals	Sodium bicarbonate	Sigma-Aldrich	S6014
Chemicals	Sodium chloride	Sigma-Aldrich	S9888
Chemicals	Sodium phosphate, monobasic	Sigma-Aldrich	S075
Chemicals	D-sucrose	Fisher BioRea-gents	BP220-212
Chemicals	TES	Sigma-Aldrich	T5691
Chemicals	Trehalose-dihydrate	Sigma-Aldrich	T0167
Chemicals	Triton X-100	Sigma-Aldrich	X100
Chemicals	Vectashield Antifade mounting medium	Vector Labora-tories	H-1000
Chemicals	All trans-retinal	Sigma-Aldrich	R2500-1G
Chemicals	All trans-retinal	Spectrum Chemical Mfg. Co.	R3041-1GM
Software, algo-rithms	Brian2 python neural network simulator software	Stimberg *et al.* 2019[47]	https://bri-ansimula-tor.org/

Software, algorithms	Fiji software	Schindelin *et al.* 2012[48]	https://fiji.sc/
Software, algorithms	*Drosophila* connectome simulator software	Shiu *et al.* 2024[34]	https://github.com/phil-shiu/Drosophila_brain_model
Software, algorithms	GraphPad Prism 10 software	GraphPad software	https://www.graphpad.com/features
Software, algorithms	MATLAB R2024a software	The Mathworks, Inc.	https://www.mathworks.com/
Software, algorithms	PyCharm Community Edition IDE software	JetBrains, Inc.	https://www.jetbrains.com/pycharm/
Software, algorithms	Python programming language software	Python Software Foundation	https://www.python.org
Software, algorithms	BioRender	BioRender	https://biorender.com
Drosophila medium	Nutri-fly Molasses Formulation (MF) fly medium	Genesee Scientific	https://geneseesci.com/
Equipment	FlyPAD and OptoPAD high throughput feeding assay	Itskov *et al.* 2014[18,19]	https://flypad.rocks/
Equipment	Modular In-vivo Multiphoton Microscopy System (MIMMS) v2.0	Janelia Research Campus, HHMI	https://www.janelia.org/open-science/mimms-22-2024

Fly stocks and culture

Drosophila melanogaster stocks (listed in key resources table) were raised at 25°C and 50%-60% relative humidity on commercially prepared standard media (cornmeal/agar/molasses/yeast; Nu-tri-Fly MF) for anatomical and 'Con-Ex' feeding experiments. For optogenetic behavioral and *ex vivo* functional imaging experiments, flies were raised under constant darkness at 25°C and 50%-60% relative humidity on the same media supplemented with 0.2 mM all trans-retinal. Flies were collected 0-3 days post-eclosion on media containing 0.4 mM all trans-retinal. Flies for anatomical and behavioral assays were 4- to 7-days-old at the time of experiments; flies used for *ex vivo* functional connectivity calcium imaging were 2- to 5-days-old at the time of dissection.

Behavioral assays

Positional preference

Positional preference assays were performed at 25°C, 50%-60% relative humidity in darkness. Female flies (3-7d old) were loaded into rectangular chambers, 8 flies per chamber. After a 2-min baseline period, one side of the chamber (selected at random) was illuminated by 0.5 Hz 1-second pulsed 625-nm red LED at designated light intensity (indicated in figure legends) for 3 min. Following the illumination period, there was a 2-min recovery period. Experiments were recorded with infrared cameras (BlackFly USB3 camera, Teledyne vision solutions). The frequencies and intensities of LED stimulation were controlled using MATLAB (MathWorks, Inc.). Acquired video was analyzed with custom MATLAB scripts that detected the position of the flies, allowing for the calculation of a Preference Index as the average difference in the fractions of flies on illuminated versus unilluminated sides[14] .

Associative learning

Associative learning assays were performed with optogenetic stimulation and was conducted in a circular arena that couples optogenetic stimulation with an odor delivery system, as described in Aso *et al.,* 2014[12] . All tests were performed at 25°C, 50%-60% relative humidity. The olfactory cues used were 4-methylcyclohexanol (1:1000) and 3-octanol (1:1000). Optogenetic stimulation used a 0.5 Hz 625-nm LED light at designated intensity (indicated in figure legends). In optogenetic

learning assay, flies were trained as groups of 12-14 individuals using a single training session consisting of 1-min exposure to air, followed by a 1-min exposure to odor A (CS+) paired with neuronal activation/silencing, followed by a 1-min exposure to air, and finally a 1-min exposure to odor B. Memory was tested 1 min after training, during which the odors A and B were delivered to each pair of opposing quadrants. Experiments were recorded under IR illumination with a camera (Point Gray Research) located above the chamber and equipped with an IR long-pass filter. The subsequent video was analyzed with custom MATLAB scripts that detect the position of flies within the chamber. A Performance Index for odor A (paired with LED, CS+) is the average difference in the fractions of flies on the odor-A versus odor-B quadrants. A reciprocal group received odor B as CS+ (paired with LED) to counterbalance flies' intrinsic odor bias. The final Performance Index is the mean of PI(A-CS+) and PI(B-CS+).

In the sugar olfactory learning assay, flies were wet-starved for 24-30 hours before training. In a training tube with filter paper without sucrose, odor A was delivered for 2 minutes, followed by 1 minute airflow. Flies were then transferred to a tube with filter paper containing sucrose, and odor B was delivered for 2 minutes (paired with sugar), followed by a 1-minute clear. Flies were transferred to the circular arena and tested for 2 minutes with odors A and B from opposite quadrants. The PI was computed as in (C), averaging the two reciprocal groups.

Proboscis extension reflex (PER)

PER assays were performed at 25°C, 50%-60% relative humidity in darkness. Mated female flies (3-7 days old) were immobilized on a coverslip using nail polish and allowed to recover for 3–4 hours in a humid chamber. Flies were then placed on a 625-nm LED panel and exposed to optogenetic activation at varying light intensities. Reactions were recorded with a USB camera and scored manually. Only complete PERs, defined as full extension of the proboscis, were counted.

Consumption-Excretion feeding

To quantify long-term feeding, we used an assay generally based on the 'Con-Ex' protocol described by Shell *et al.,* 2018[49] . Dyed food was prepared via the addition of FD&C blue No. 1 dye to normal fly food with a concentration of 1% (wt/vol). A small volume of dyed food (100 µL) was

pipetted into the underside of a 2.0 mL Eppendorf tube cap 30 min prior to adding flies. Two holes were poked near the top of the vials using a heated needle, allowing air/moisture circulation. Two 3- to 7-days-old mated female flies were transferred and allowed to feed *ad libitum* in the vials for 24 h at 25°C (55% humidity). After feeding, vials were placed on dry ice to euthanize the flies, which were then transferred to a 1.7 mL Eppendorf tube. Fly carcasses were ground in 300 µL of distilled water and centrifuged. A portion of supernatant (100 µL) was transferred to a 96-well culture plate. Concurrently, the excreta in the feeding vial were dissolved in 500 µL of distilled water, vortexed for 5-10 s, and 100 µL of the sample transferred to the same 96-well culture plate. Using a plate reader, the absorbance values of the samples (λ = 620 nm) were measured and converted to concentrations via standard curves, then converted to usable mass for data analysis.

FlyPad/OptoPad feeding

This assay was quantified by use of the FlyPad behavioral monitoring system[18,19] , at 25°C, 50% - 60% relative humidity. Warmed liquified media was loaded into both probes in each FlyPAD chamber in darkness. Individual female flies (3-7 d old) were placed in each FlyPAD chamber and were allowed to feed *ad libitum* for 50 min total. In the open-loop feeding and choice assay, the FlyPAD chambers were illuminated with 625-nm red LEDs to optogenetically stimulate channelrhodopsin-expressing neurons. In the closed-loop feeding assay, the FlyPAD chambers were only illuminated with red LED when flies fed on one of the two probes in each arena. The probe associated with illumination was alternated for the next set of experiments to mitigate potential probe-specific bias. Media containing 7% yeast, 160 mM sucrose, and 0.7% agar was used for open-loop feeding assay. Media containing either 0.7% agar (neutral taste), 100 mM sucrose (sweet taste), or 0.5 mM quinine (bitter taste) were used for open-loop choice assays and closed-loop feeding assays. Detailed recipe in Table S1. Analysis of feeding behavior used custom MATLAB scripts that extracted the total number of sips during the feeding period.

Immunostaining and confocal imaging

Immunohistochemical staining and imaging were performed as previously described (Shao *et al.,* 2019)[50] . Briefly, brains were dissected in cold Schneider's Insect (S2) medium, fixed in 2% paraformaldehyde in S2 at Room Temperature (RT) under nutation for 55-65 min in covered Eppendorf tubes, washed 3-4 times with PBT0.5 (phosphate buffered saline, PBS, containing 0.5% Triton X-100) at RT, blocked with PAT3 (1xPBS, 1g/100mL BSA, 0.5% Triton X-100) for 1 hour at RT, incubated with primary antibody (1:500 rabbit anti-GFP, 1:50 mouse anti-nc82 in PAT3) at 4°C overnight, washed 3-4 times in PBT0.5, incubated with secondary antibody (1:500 Alexa 488 anti-rabbit, 1:500 Alexa 568 anti-mouse in PAT3) at 4°C overnight, washed with PBT0.5 and PBS, and mounted in Vectashield. The brains were then imaged on a confocal microscope (Zeiss CellDiscoverer 7, using Zen Blue software).

Ex vivo calcium imaging

All functional imaging was performed on 2- to 5-day-old female flies. Whole brains were dissected in a Sylgard silicone elastomer (Dow Inc.) coated dish, immersed in artificial fly hemolymph (103 mM NaCl, 3mM KCl, 2 mM $CaCl_2$, 4 mM $MgCl_2 \cdot 6\ H_2O$, 26 mM $NaHCO_3$, 1 mM NaH_2PO_4, 8 mM trehalose, 10 mM glucose, 5 mM TES, bubbled with 95% O_2/5% CO_2). Brains were placed on a poly-Lysine coated coverslip and imaged with a resonant-scanning 2-photon microscope (MIMMS v2.0, Janelia Research Campus), using a laser with a 920 nm excitation wavelength (Toptica Femto-Fiber Ultra 920) and an excitation power of 19-33 mW (2.7-4.3 mW/mm^2 intensity). Emitted fluorescence was detected with GaAsP photomultiplier tubes (Hamamatsu) controlled via a Janelia PMT Controller. Images were acquired with an Olympus × 40 water-dipping, 0.8 numerical aperture objective at 512 pixels × 512 pixels resolution. Optogenetic stimulation of CsChrimson was provided by a 660-nm red light LED diode (ThorLabs M660L4), fed into a digital mirror device (Texas Instruments DLP Lightcrafter 4500) and projected through the objective. Photostimulation consisted of 4 x 1 s pulses, separated by a 24 s inter-pulse interval, with a stimulation power of 20-21 µW (2.8-3.0 µW/mm^2 intensity). Volume stacks were continuously imaged at 2x magnification, and consisted of 45 slices, with an inter-slice interval of 2 µm, thus allowing all the PAM-DANs compartments to be imaged. Stack acquisition began 10s prior to the 1st LED pulse and

stopped 24s after the termination of the final pulse. After optogenetic stimulation, brains were imaged for ROI definition of mushroom body compartment anatomy using the same imaging stack dimensions as above, using both 920 nm, and 1050 nm excitation (Toptica FemtoFiber Ultra 1050). Then power intensity for imaging at the 920- and 1050-nm excitation was 3.2-3.4 and 3.1-3.2 mW/mm^2 respectively.

Regions of interest (ROI)s for each brain were drawn using custom MATLAB software and the 1050 nm anatomy images described above. The average pixel intensity for each ROI ($fluor_{avg}$) was calculated, as was its average baseline intensity ($fluor_{bseln}$), defined as the averaged intensity for the 5 volumes (approximately 1.5 s) acquired immediately prior to each optogenetic pulse onset. Average background intensity ($fluor_{bckgr}$) for each volume was calculated from a ROI located in non-brain-tissue containing space. For each PAM compartment, ΔF/F was calculated using the formula:

$$\frac{(fluor_{avg}(t) - fluor_{bckgr}(t)) \; - \; (fluor_{bseln}(t) \; - \; fluor_{bckgr}(t))}{(fluor_{bseln}(t) \; - \; fluor_{bckgr}(t))}$$

Connectome simulation

Digital experiments were performed using a Python-based *Drosophila melanogaster* neural simulation, described previously[34] , implemented using the open-source Brian2 library[47] . The default model parameters described by Shiu *et al.* 2024 were used: 1000 ms trial duration, 30 trial repetitions, −52 mV resting potential, −52 mV reset potential after a spike, −45 mV spiking threshold, 2.2 ms refractory period, 5 ms tau for synapse decay, 1.8 ms time delay from spike to change in membrane potential. The free parameter model synaptic weight (W_{syn}) was adjusted to achieve differing levels of propagation of GRN activation throughout the connectome. Labellar sugar gustatory neurons (GRN), second- and third-order gustatory interneurons (GINs), and fox neurons were stimulated using Poisson distributed input at stimulation rates from 10-200 Hz. A downstream neuron was considered activated if its average firing rate was non-zero during stimulation of any of the simulated experiments. Experiments were executed in Python, using the PyCharm

Community Edition IDE, and the output (mean spiking rate tables of activated connectome neurons) were used for further analysis and visualization using custom MATLAB scripts (The MathWorks, Inc).

Statistical analysis

Analyses were performed at the level of the experimental unit. For single-fly assays, the unit of analysis was the individual fly, such that each fly contributed one value (thus N = number of flies). For group assays (e.g., arena-based population tests), the unit of analysis was an independently loaded cohort of flies tested together in a single chamber/arena; all flies in that cohort were aggregated to yield one summary value (e.g., PI or total sips), and that value contributed $N = 1$. In these group assays, the number of flies per cohort (n) is reported descriptively in figure legends but was not used for statistical inference to avoid pseudo-replication. When cohorts were measured more than once under different conditions, within-cohort comparisons were analyzed with paired tests; otherwise, unpaired tests were used across independent cohorts.

For each dataset (and, where applicable, model residuals for >2-group designs), distributional normality was assessed with the Shapiro–Wilk test ($\alpha = 0.05$). All hypothesis tests were two-tailed. When the normality criterion was met, two-group comparisons used paired or unpaired t-tests as appropriate to the design, and >2-group comparisons used one-way ANOVA followed by Tukey's multiple-comparisons test. When the normality criterion was not met, the behavioral index (such as $(Sip_{ON} - Sip_{OFF})/Sip_{Total}$) was tested against 0 using a one-sample Wilcoxon signed-rank test; within-fly ON versus OFF probe counts were compared with the Wilcoxon matched-pairs signed-rank test; two-genotype comparisons used the Mann–Whitney U test; and >2-genotype comparisons used the Kruskal–Wallis test with Dunn's post hoc multiple-comparisons procedure.

The exact test used, sample size (n), and two-tailed p-values are provided in the figure legends. Analyses were performed in GraphPad Prism.

1 **Figures and Figure legends**

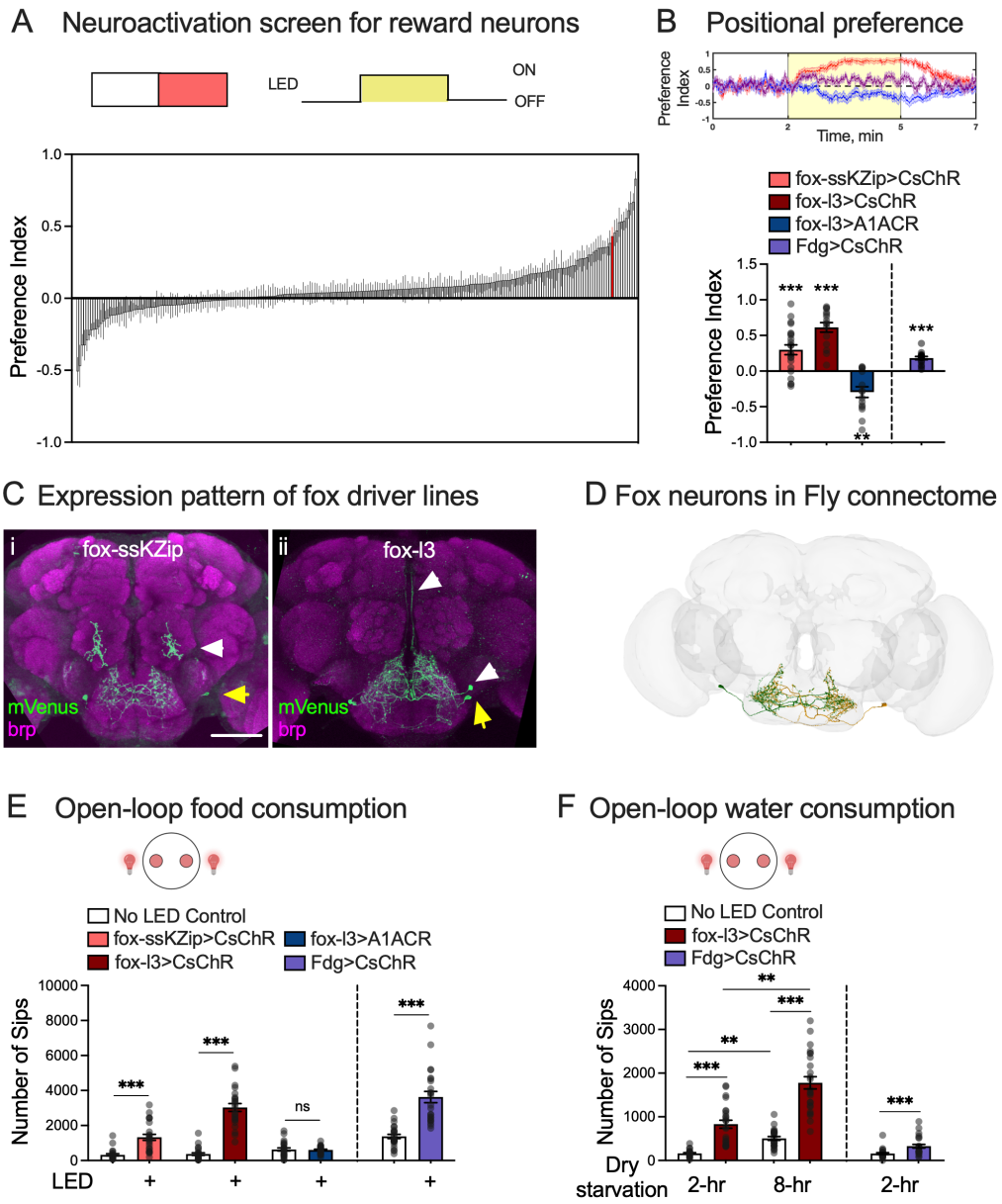

2

3 **Figure 1. Activating a pair of SEZ interneurons, called Fox, is sufficient to drive appetitive be-**

4 **haviors in flies.**

5 A. Results of a screen for neurons whose activation is rewarding or aversive to flies using a posi-

6 tional preference assay[14] . A preference index greater than 0 indicates attraction; lower than 0

7 indicates avoidance. Data from mated female flies are shown. The performance of fox-

ss1>CsChrimson in the screen is highlighted in red. N = 10 replicates for each driver line. Each replicate contains 6-8 flies. LED intensity: 11.5 mW/cm^2.

B. Flies preferred the illuminated side in the positional preference assay when their Fox neurons were optogenetically activated by CsChrimson (denoted as CsChR in figures) driven by fox-ssKZip and fox- l3. In fox-ssKZip (fox-ss1 ∩ TH-D-KZip), PPM3 neurons are excluded by expressing 'killer zipper' in specific dopaminergic neurons including those in the PPM3 cluster (TH-D-KZip[42]), which prevents split-GAL4 AD/DBD heterodimerization and thereby suppresses expression specifically in PPM3. Fox-l3 is a new split-GAL4 driver[14]. Both drivers isolated the same pair of neurons in SEZ, which we identified as Fox neurons. Flies avoided the illuminated side when their Fox neurons were blocked by the chloride transporter A1ACR. Like Fox neurons, activating a command neuron for feeding, the third-order gustatory interneuron Fdg neurons[20,21] (Fdg>CsChrimson), induced positional preference. N = 22 for fox-ssKZip>CsChrimson; N = 15 for Fox-l3>CsChrimson; N = 15 for fox-l3>A1ACR; N = 15 for Fdg>CsChrimson. Each replicate contains 6-8 flies. One-sample *t* test (hypothetical value = 0), ** $p<0.01$, *** $p<0.001$. LED intensity: 11.5 mW/cm^2. Representative traces of flies' performance (fox-l3>CsChrimson in red, Fdg>CsChrimson in purple, and fox-l3>A1ACR in blue) are shown in the upper panel.

C. Immunostaining of CsChrimson-mVenus driven by fox-ssKZip (i) and fox-l3 (ii) driver lines that label Fox neurons: (i) fox-ssKZip; (ii) fox-l3. Yellow arrows indicate Fox neurons; white arrows indicate non-Fox neurons labeled by the same driver. mVenus signal and brp (neuropils) were revealed by anti-GFP (green) and nc82 (magenta) antibody staining, respectively. Scale bar: 50 μm.

D. Fox neurons' morphology in the FlyWire connectome (the Female Adult Fly Brain, FAFB).

E. Activating Fox neurons with CsChrimson using fox-ssKZip and fox-l3 driver lines increased food (7% yeast and 160 mM sucrose) consumption in fed flies; however, blocking Fox neurons with A1ACR did not affect feeding. Similarly, activating Fdg neurons (Fdg>CsChrimson) increased food consumption in fed flies. N = 24 flies for each group. Mann Whitney test for fox-ssKZip>CsChrimson, fox-l3>CsChrimson and respective no LED controls, *** $p<0.001$. *t* test for fox-l3>A1ACR, Fdg>CsChrimson, and respective no LED controls, ns $p>0.05$, *** $p<0.001$. LED intensity: 12 mW/cm^2.

F. Activating Fox neurons (fox-l3>CsChrimson) significantly increased water consumption when flies were dry-starved for 2 hours and 8 hours. N = 24 flies for each group. Kruskal-Wallis test and Dunn's multiple comparisons test, ** $p<0.01$, *** $p<0.001$. Activating the third-order gustatory interneuron Fdg neurons (Fdg>CsChrimson) also increased water consumption in flies with 2-hr dry-starvation. N = 24 flies for each group. *t* test (no LED and LED groups of the same genotype), *** $p<0.001$. LED intensity: 12 mW/cm^2.

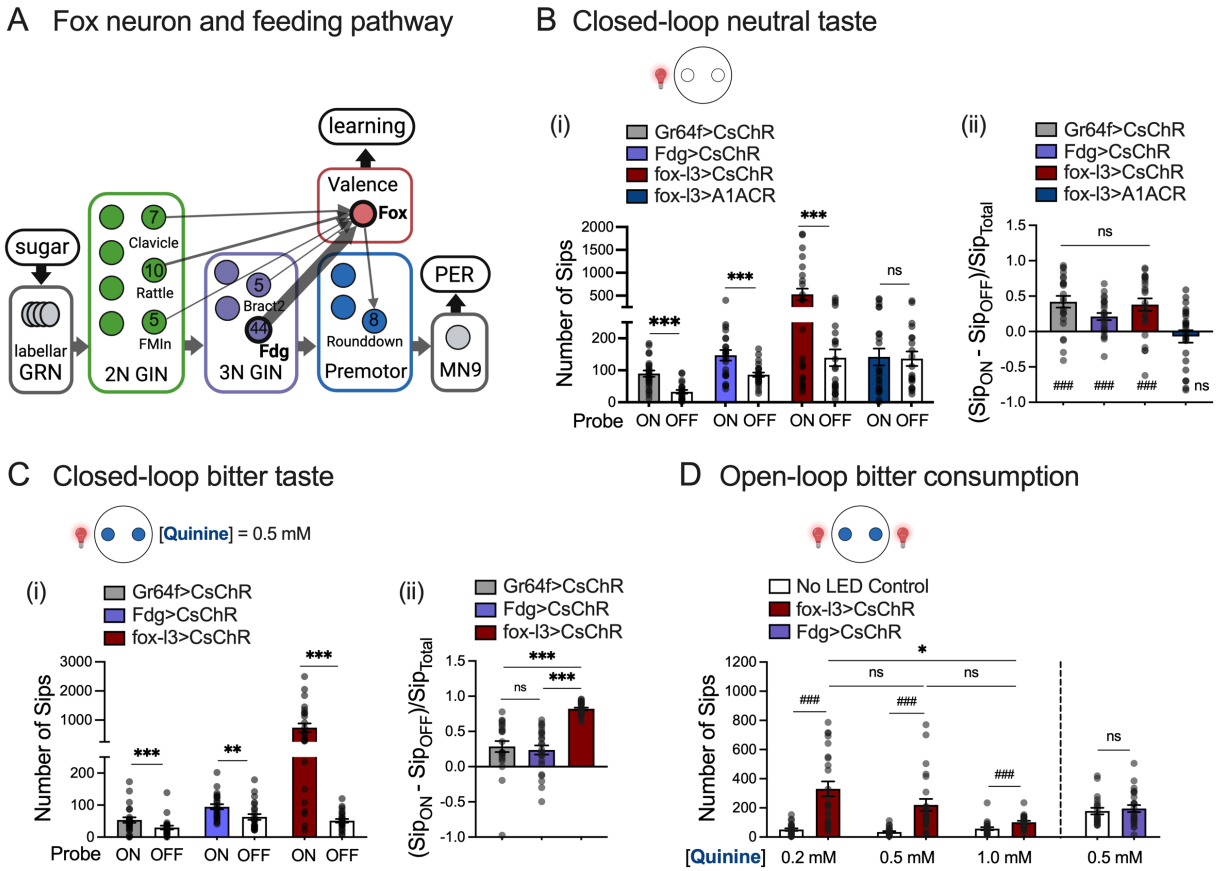

Figure 2. Activation of Fox neurons overrides the intrinsic valence of neutral and aversive taste.

A. Illustration of Fox neural connections with the neural pathways that regulate proboscis extension reflex (PER), modified from Shiu et al.[21] . The number of synapse counts onto Fox neurons is indicated in the circle that represents corresponding neurons presynaptic to Fox. Synapses from Fdg neurons comprise 10% of the synaptic inputs to Fox neurons.

B. Optogenetic activation of either Gr64f-expressing GRNs (Gr64f>CsChR), Fdg neurons (Fdg>CsChR), or Fox neurons (fox-l3>CsChR) during feeding on one of the two probes containing agar significantly increased flies' feeding from the associated probe, whereas optogenetic silencing of Fox neurons (fox-l3>A1ACR) with a probe did not change the flies' choice. The y-axis is segmented to highlight the low sip numbers in Gr64f and Fdg flies. Panel (i) shows the number of sips on each probe. Wilcoxon matched-pairs signed rank test on sips from LED associated (ON) and non-associated (OFF) probes of individual genotype, ns. p>0.05; *** p<0.001. Panel (ii) shows

feeding preference, calculated as the difference in sips on associated versus non-associated probe, normalized by the total sips from both probes ($(Sip_{ON} - Sip_{OFF})/Sip_{Total}$). Flies were wet-starved 24 hours before experiments. LED intensity: 12 mW/cm^2 for Fox and Fdg neuronal activation; 6 mW/cm^2 for Gr64f neuronal activation. Wilcoxon signed rank test against a hypothetical value of 0 on individual genotype, ### $p<0.001$, ns $p>0.05$. Kruskal-Wallis test, followed by Dunn's multiple comparisons test, across genotypes, ns $p>0.05$. N = 24 flies for each group.

C. Flies' feeding from one of the two probes containing quinine (0.5 mM) was significantly increased when the probe was associated with Fox activation (fox-l3> CsChrimson), but not with Gr64f-expressing GRN (Gr64f> CsChrimson) or with Fdg neuron (Fdg> CsChrimson) activation. The y-axis is segmented to highlight the low sip numbers in Gr64f and Fdg flies. Panel (i) shows the number of sips on each probe. Wilcoxon matched-pairs signed rank test on sips from LED-associated (ON) and non-associated (OFF) probes of individual genotype, ** $p<0.01$, *** $p<0.001$. Panel (ii) shows feeding preference, calculated as the difference in sips on associated versus non-associated probe, normalized by the total sips from both probes ($(Sip_{ON} - Sip_{OFF})/Sip_{Total}$). Kruskal-Wallis test, followed by Dunn's multiple comparisons test, across genotypes, ns $p>0.05$, *** $p<0.001$. N = 24 flies for each group. Flies were wet-starved 24 hours before experiments. LED intensity: 12 mW/cm^2 for Fox and Fdg neuronal activation; 6 mW/cm^2 for Gr64f neuronal activation.

D. Activating Fox neurons (fox-l3>CsChrimson) significantly increased flies' consumption of agar containing 0.2 mM and 0.5 mM quinine but did not promote consumption for agar containing 1.0 mM quinine. N=24 flies for each group. Wilcoxon matched-pairs signed rank test, ns $p>0.05$, ### $p<0.001$, on sips from LED-associated and non-associated probes of dividual quinine concentration. Kruskal-Wallis test, followed by Dunn's multiple comparisons test, across quinine concentrations, ns $p>0.05$, * $p<0.05$. In contrast, activating Fdg neurons (Fdg>CsChrimson) did not increase the consumption of quinine (0.5 mM). N = 24 flies for each group. Wilcoxon matched-pairs signed rank test, ns $p>0.05$, on NO-LED and LED conditions. Flies were fed before experiments. LED intensity: 12 mW/cm^2.

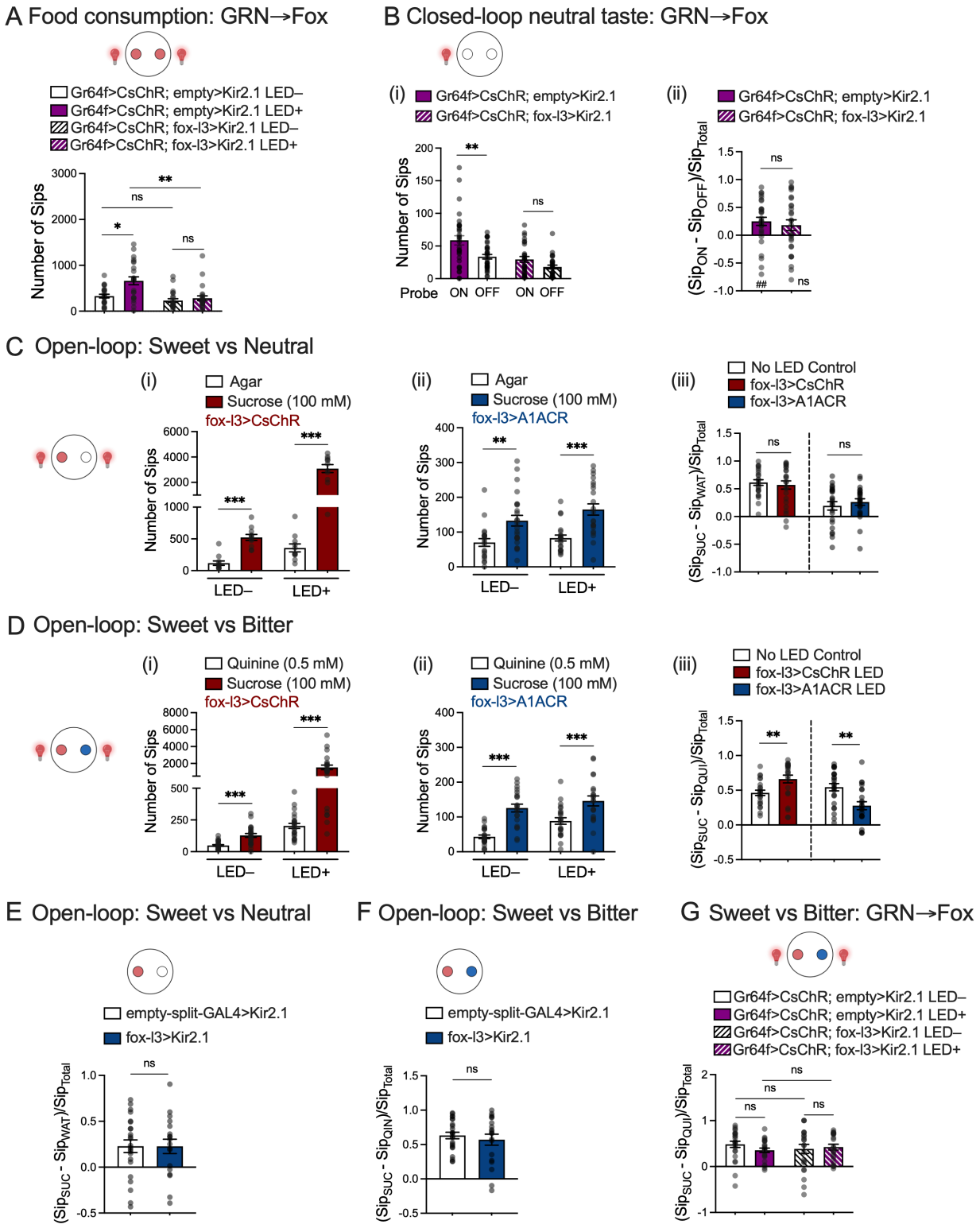
A Food consumption: GRN→Fox
Gr64f>CsChR; empty>Kir2.1 LED–
Gr64f>CsChR; empty>Kir2.1 LED+
Gr64f>CsChR; fox-l3>Kir2.1 LED–
Gr64f>CsChR; fox-l3>Kir2.1 LED+
Number of Sips
B Closed-loop neutral taste: GRN→Fox
(i)
Gr64f>CsChR; empty>Kir2.1
Gr64f>CsChR; fox-l3>Kir2.1
Number of Sips
Probe ON OFF ON OFF
(ii)
Gr64f>CsChR; empty>Kir2.1
Gr64f>CsChR; fox-l3>Kir2.1
(Sip_ON - Sip_OFF)/Sip_Total
C Open-loop: Sweet vs Neutral
(i)
Agar
Sucrose (100 mM)
fox-l3>CsChR
Number of Sips
LED– LED+
(ii)
Agar
Sucrose (100 mM)
fox-l3>A1ACR
Number of Sips
LED– LED+
(iii)
No LED Control
fox-l3>CsChR
fox-l3>A1ACR
(Sip_SUC - Sip_WAT)/Sip_Total
D Open-loop: Sweet vs Bitter
(i)
Quinine (0.5 mM)
Sucrose (100 mM)
fox-l3>CsChR
Number of Sips
LED– LED+
(ii)
Quinine (0.5 mM)
Sucrose (100 mM)
fox-l3>A1ACR
Number of Sips
LED– LED+
(iii)
No LED Control
fox-l3>CsChR LED
fox-l3>A1ACR LED
(Sip_SUC - Sip_QUI)/Sip_Total
E Open-loop: Sweet vs Neutral
empty-split-GAL4>Kir2.1
fox-l3>Kir2.1
(Sip_SUC - Sip_WAT)/Sip_Total
F Open-loop: Sweet vs Bitter
empty-split-GAL4>Kir2.1
fox-l3>Kir2.1
(Sip_SUC - Sip_QIN)/Sip_Total
G Sweet vs Bitter: GRN→Fox
Gr64f>CsChR; empty>Kir2.1 LED–
Gr64f>CsChR; empty>Kir2.1 LED+
Gr64f>CsChR; fox-l3>Kir2.1 LED–
Gr64f>CsChR; fox-l3>Kir2.1 LED+
(Sip_SUC - Sip_QUI)/Sip_Total

82

Figure 3. Silencing Fox neurons impairs taste valence without changing recognition of taste identity.

A. Optogenetic activation of Gr64f neurons (Gr64f-LexA>LexAop-CsChrimson; empty>UAS-Kir2.1) promoted feeding. In contrast, blocking Fox neurons with Kir2.1 (Gr64f-LexA>LexAop-CsChrimson; fox-l3>UAS-Kir2.1) suppressed the enhanced food consumption caused by Gr64f activation. LED intensity: 6 mW/cm^2. N = 24 flies for each group. Kruskal-Wallis test, followed by Dunn's multiple comparisons test, ns. p>0.05; * p<0.05, ** p<0.01.

B. Panel (i): Activating Gr64f neurons (Gr64f-LexA>LexAop-CsChrimson; empty>UAS-Kir2.1) increased number of sips from the agar probe paired with activation, whereas silencing Fox neurons (Gr64f-LexA>LexAop-CsChrimson; fox-l3>UAS-Kir2.1) abolished this increase. Wilcoxon matched-pairs signed rank test, ns p>0.05, ** p<0.01. Panel (ii): Flies showed preference (calculated as (Sip_{ON} - Sip_{OFF})/Sip_{Total}) for the associated probe without Fox silencing, whereas the preference for associated probe was not different from 0 in flies with Fox silenced. Wilcoxon signed rank test against a hypothetical value of 0 on individual genotype, ns p>0.05, ## p<0.01. However, the two genotypes were not statistically different when tested in Mann-Whitney test across genotypes, ns. p>0.05. N = 28-30 flies for each group. LED intensity: 6 mW/cm^2.

C. Panels (i-ii): Flies took more sips from the sucrose-containing probe than the agar-containing probe whether Fox neurons were activated (fox-l3>CsChrimson) or silenced (fox-l3>A1ACR). Wilcoxon matched-pairs signed rank test, *** p<0.001. Panel (iii): Manipulating Fox neuronal activity did not alter sucrose-agar discrimination: flies' preference for sucrose (calculated as (Sip_{SUC}-Sip_{WAT})/Sip_{Total}) was unchanged. Mann-Whitney test, ns. p>0.05. [sucrose] = 100 mM. N = 24 flies for Fox activation groups and N = 23 flies for Fox silencing groups. LED intensity: 12 mW/cm^2.

D. Panels (i-ii): Flies took more sips from the sucrose-containing probe than the quinine-containing probe whether Fox neurons were activated (fox-l3>CsChrimson) or silenced (fox-l3>A1ACR). Wilcoxon matched-pairs signed rank test, *** p<0.001. Panel (iii): Optogenetically activating Fox neurons increased preference for sucrose over quinine (calculated as (Sip_{SUC}-Sip_{QUI})/Sip_{Total}), while blocking Fox neurons decreased the preference. Mann-Whitney test, ** p<0.01. [sucrose] = 100 mM, [quinine] = 0.5 mM. N = 23 flies for each group. LED intensity: 12 mW/cm^2.

111 E. Constitutively blocking Fox neurons with Kir2.1 (fox-l3>Kir2.1) did not alter flies' preference for
112 sucrose over agar (calculated as (Sip_{SUC}-Sip_{WAT})/Sip_{Total}). Mann-Whitney test, ns. $p>0.05$. [sucrose]
113 = 100 mM. N = 23 flies for genetic control group and N = 18 flies for Fox silencing group.

114 F. Constitutively blocking Fox neurons with Kir2.1 (fox-l3>Kir2.1) did not alter flies preference for
115 sucrose over quinine (calculated as (Sip_{SUC}-Sip_{QUI})/Sip_{Total}). Mann-Whitney test, ns. $p>0.05$. [su-
116 crose] = 100 mM, [quinine] = 0.5 mM. N = 23 flies for genetic control group and N = 19 flies for
117 Fox silencing group.

118 G. Optogenetic activation of Gr64f-expressing sweet gustatory receptor neurons with (Gr64f-
119 LexA>LexAop-CsChrimson; fox-l3>UAS-Kir2.1, N = 24 flies for each group) or without silencing Fox
120 neurons (Gr64f-LexA>LexAop-CsChrimson; empty>UAS-Kir2.1, N=23 flies for no LED control and
121 N=22 flies for LED group) did not change flies' preference for sucrose over quinine. Kruskal-Wallis
122 test, followed by Dunn's multiple comparisons test, ns. $p>0.05$. LED intensity: 6 mW/cm^2.

123

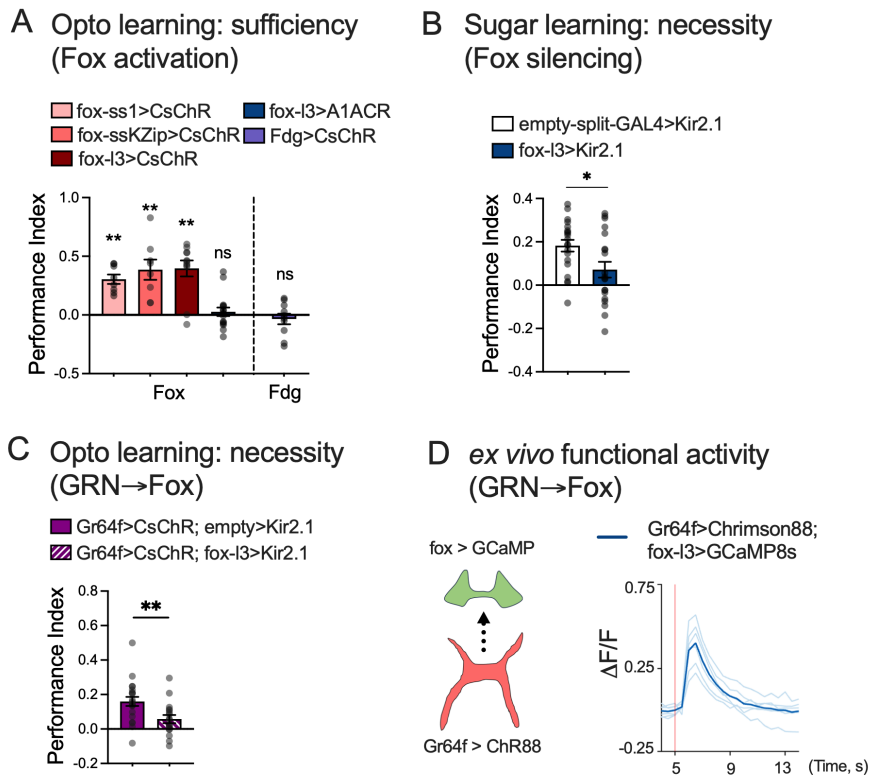

Figure 4. Fox neurons are essential for appetitive learning mediated by GRN activation.

A. Flies formed appetitive memory with Fox activation by fox-ss1, fox-ssKZip and fox-l3 drivers. Blocking Fox neurons resulted in no memory formation. Unlike Fox neurons, pairing the activation of Fdg neurons (Fdg>CsChrimson) with odors did not generate appetitive or aversive learning. N = 8 for fox-ss>CsChrimson and fox-ssKZip>CsChrimson; N = 11 for fox-l3>CsChrimson; N = 16 for fox-l3>A1ACR; N = 20 for Fdg>CsChrimson. Each replicate is an average of two experiments with reciprocal odor-LED pairs. Each experiment (half N) contains 12-14 flies. Wilcoxon signed rank test against hypothetical value of 0, ** $p<0.01$, ns. $p>0.05$. LED intensity: 11.5 mW/cm^2.

B. Flies formed appetitive memory with odors paired with sucrose. Blocking Fox neurons resulted in decreased memory formation. N = 20. Each replicate is an average of two experiments with reciprocal odor-sucrose pairs. Each experiment (half N) contains 12-14 flies. Flies were wet-starved for 24-30 hours. Unpaired *t* test, * $p<0.05$.

138 C. Optogenetic activation of Gr64f-expressing sweet gustatory receptor neurons (Gr64f-
139 LexA>LexAop-CsChrimson; empty>UAS-Kir2.1) formed appetitive memory when paired with
140 odors (N = 21). In contrast, blocking Fox neurons with Kir2.1 (Gr64f-LexA>LexAop-CsChrimson;
141 fox-l3>UAS-Kir2.1) suppressed the learning formed by Gr64f activation (N = 17). Each replicate is
142 an average of two experiments with reciprocal odor-LED pairs. Each experiment (half N) contains
143 12-14 flies. *t* test, ** $p<0.01$. LED intensity: 6 mW/cm^2.

144 D. Left panel: Illustration of the *ex vivo* functional connectivity experiment. We activated Gr64f-
145 expressing neurons while collecting calcium signals from the projections of Fox neurons. Right
146 panel: Optogenetically stimulating Gr64f-expressing neurons led to significant calcium response
147 in Fox neurons. ΔF/F of individual sample is shown with light blue traces; the mean ΔF/F of all
148 samples is shown with a dark blue trace. Genotype: Gr64f-LexA>LexAop-Chrimson88-tdTomato;
149 Fox-l3>UAS-RSET-GCaMP8s. N =6 flies.

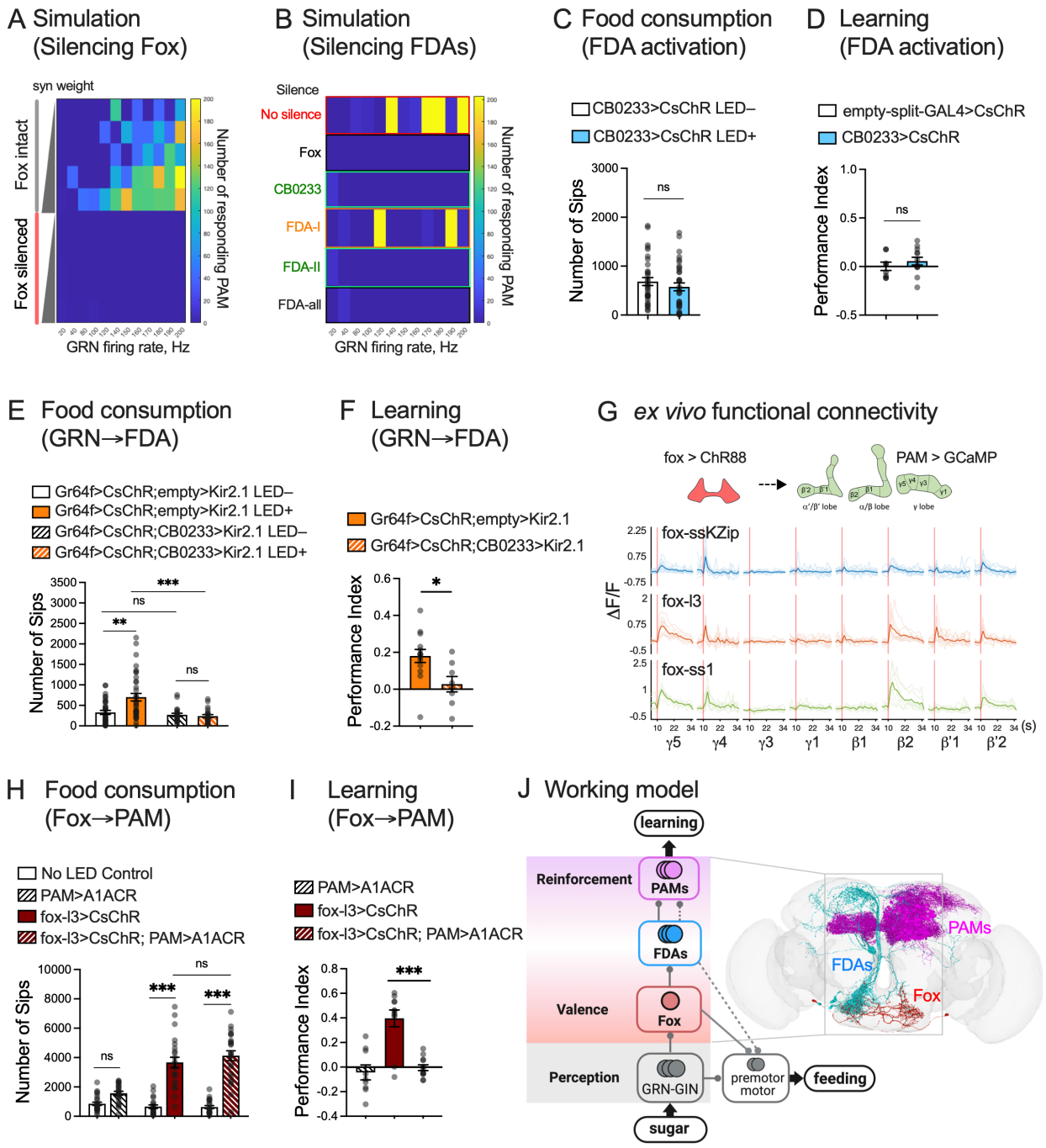

Figure 5. Fox neurons relay GRN signals to PAM dopaminergic neurons through downstream ascending neurons.

A. Heatmap of the number of PAM-DANs that respond to the stimulation of unilateral GRNs and GINs, with and without Fox neurons blocked, at various model synaptic weights (0.37, 0.38, 0.382, 0.386, 0.39 mV) and GRN firing rates (20, 40, 80, 100, 120, 140, 150, 160, 170, 180, 190, 200 Hz)

156 in computational simulation. Each number of responsive neurons is an average of five simulation
157 trials with the same parameters.

158 B. Heatmap of the number of PAM-DANs that respond to the stimulation of unilateral GRNs and
159 GINs, with and without Fox and FDAs blocked (model synaptic weight = 0.39). FDA-I neurons (or-
160 ange) synapse directly onto PAM-DANs. FDA-II neurons (green) do not synapse directly on PAM-
161 DANs. CB0233 is an FDA-II cell type with the most synapses with Fox neurons.

162 C-D. Optogenetic activation of CB0233 (CB0233>CsChrimson), a pair of FDA-II neurons, did not
163 enhance food consumption (C, N = 36 flies for each group, Mann-Whitney test, ns. $p>0.05$) or
164 generate appetitive memory when paired with odors (D, N = 8 for empty and N = 12 for CB0233.
165 Each replicate is an average of two experiments with reciprocal odor-LED pairs. Each experiment
166 (half N) contains 12-14 flies. *t* test, ns. $p>0.05$).

167 E-F. Blocking CB0233 neurons (FDA-II) with Kir2.1 (Gr64f-LexA>LexAop-CsChrimson;
168 CB0233>UAS-Kir2.1) suppressed the enhanced feeding (E, N = 24-36 flies, Kruskal-Wallis test, fol-
169 lowed by Dunn's multiple comparisons test, ns. $p>0.05$, ** $p<0.01$, *** $p<0.001$) and learning (F,
170 N = 14 and 8. Each replicate is an average of two experiments with reciprocal odor-LED pairs. Each
171 experiment (half N) contains 12-14. *t* test, * $p<0.05$) induced by Gr64f activation. LED intensity: 6
172 mW/cm^2 for feeding assay and learning assay.

173 G. Upper panel: Illustration of the *ex vivo* functional connectivity experiment. We activated Fox
174 neurons while collecting calcium signals from the axons of PAM-DANs that innervate various
175 mushroom body compartments. Lower panel: Optogenetically stimulating Fox neurons with three
176 Fox drivers led to compartment-specific activation in PAM dopaminergic neurons. Genotype: Fox-
177 driver>UAS-Chrimson88-tdTomato; PAM (58E02)-LexA>LexAop-GCaMP7s. $\Delta F/F$ of individual sam-
178 ple is shown with light-color traces; the mean $\Delta F/F$ of all samples is shown with dark-color traces.
179 N =13 flies for fox-ss1, N=10 flies for fox-ssKZip, and N=7 flies for fox-l3.

180 H-I. Optogenetic activation of Fox neurons while blocking PAM dopaminergic neurons with A1ACR
181 (fox-l3>UAS-CsChrimson; 58E02-LexA>LexAop-A1ACR) did not affect feeding (H, N = 24 flies for all
182 groups, Kruskal-Wallis test, followed by Dunn's multiple comparisons test, ns. $p>0.05$, ***
183 $p<0.001$) but abolished appetitive learning (I, N = 9, 12, 12. Each replicate is an average of two

experiments with reciprocal odor-LED pairs. Each experiment (half N) contains 12-14 flies. Mann-Whitney test, *** $p<0.001$). LED intensity: 12 mW/cm^2 for feeding assay and 11.5 mW/cm^2 for learning assay.

J. Working model. Fox neurons—a bilateral SEZ pair—assign and relay positive valence from sweet GRNs to PAM-DANs via ascending downstream (FDA) neurons, linking peripheral taste detection to reinforcement. The circuit forms a convergent–divergent motif with Fox as an SEZ bottleneck: multiple sweet GRNs/GINs converge onto Fox, whose outputs diverge to premotor and ascending pathways. A premotor/feeding route, dominated by SEZ interneurons plus FDA neuron CB0233, provides short-latency access to motor nodes. A parallel ascending valence route engages mushroom body–innervating PAM-DANs to drive reinforcement and appetitive memory.